Large spin gaps in the half-metals MN_4 (M=Mn, Fe, Co) with N_2 dimers

Jun Deng,[1,2] Ning Liu,[1,2] Jiangang Guo,[1,3,*] and Xiaolong Chen[1,2,3,†]

[1]*Beijing National Laboratory for Condensed Matter Physics, Institute of Physics, Chinese Academy of Sciences, Beijing 100190, China*

[2]*School of Physical Sciences, University of Chinese Academy of Sciences, Beijing 100049, China*

[3]*Songshan Lake Materials Laboratory, Dongguan, Guangdong 523808, China*

(Received 14 January 2019; revised manuscript received 15 April 2019; published 10 May 2019)

We predict that cubic MN_4 (M=Mn, Fe, Co) are all half-metals with the largest spin gap up to ∼5 eV. They possess robust ferromagnetic ground states with the highest Curie temperature up to $\sim 10^3$ K. Our calculations indicate these compounds are energetically favored, dynamically and mechanically stable. It is proposed that self-doping of these 3d transition metals occurs in MN_4 due to the reduction in electronegativity of N_2 dimers. This model can well explain the calculated integer magnetic moments, large spin gaps of MN_4, and semiconducting behavior for NiN_4 as well. Our results highlight the difference in electronegativity between transition metal ions and nonmetal entities in forming half-metals and the role of N_2 dimer in enlarging the spin gaps for nitride half-metals.

DOI: 10.1103/PhysRevB.99.184409

I. INTRODUCTION

Half-metals are a class of material that behave as metals by electrons of one spin orientation and as semiconductors by electrons of the other spin orientation [1]. They are promising candidates for spintronics applications from magnetic tunneling junctions to giant magnetoresistance devices and injecting spin-polarized currents into semiconductors [2–4]. For practical applications, ideal half-metals should be magnets having high Curie temperatures (T_c) and large enough half-metallic gaps. Previous studies identified a number of half-metals with varying T_c (∼1100 K) and gap (0.5–2 eV), including full Heusler Co_2FeSi [5], half-Heusler NiMnSb [6], oxides CrO_2 [7] and Fe_3O_4 [8], perovskites Sr_2FeMoO_6 [9], and so on, which have been intensively investigated over the last decades. The search and prediction of a new half-metal with better performance, however, are still tough tasks.

So far, all known half-metallic candidates lie in limited structural types and chemical species. They can be basically categorized into two groups: one being high-valence transition metal oxides and the other low-valence transition metal silicides or antimonides. Both groups of half-metals contain one or two transition metals centered either in tetrahedra or octahedra in their structures. Ferro- and ferrimagnetism are realized through double-exchange or superexchange interactions of spins affected by the effects of Hund's rule, crystal field, and orbital hybridization. Two channels of band structure, metallic and nonmetallic characteristics, form in terms of spin direction as the most striking feature for half-metals. In the nonmetallic channel, the valence bands (VB) are always composed of half-filled five d or three p orbital electrons, resulting in full occupation of the bands in one spin direction. These d electrons come from a single magnetic Fe ion in Sr_2MoFeO_6 [10] or two magnetic ions as Ni and Mn in Heusler NiMnSb [6]. The p orbitals usually come from oxygen in the case for CrO_2 [11]. Their conduction bands (CB) are, therefore, empty. In the metallic channel, the energy bands composed of hybrid orbitals of d metals or/and nonmetal elements cross the Fermi energy.

From an electronegative point of view, these half-metals can be regarded as formation from high valence transition metal ions and a nonmetallic element with large electronegativity, or from low-valence transition metal ions and nonmetallic elements with relative low electronegativity. In high-valence transition metals in oxides it is difficult to transfer electrons to oxygen or vice versa because of the metals' high ionization energy for the remaining electrons and large electronegativity for oxygen. So do the second group of half-metals with low-valence transition metals where the hopping of electrons are forbidden due to the weak bonding of transition metals and low-electronegative Si and Sb. If a transition metal has a proper number of electrons in its d subshell to guarantee a full occupation of VB, half-metallicity will ensue. A N_2 dimer has a lower electronegativity in comparison with atomic N as it meets the octet electron rule. Moreover, the π and π^* orbitals in the dimer may serve as the VB and CB with a large gap in the nonmetallic channel, helpful in widening the spin gaps for half-metals. This proposition deserves a test for there is no known half-metals with a dimer as its nonmetallic component up to now.

Recently, a new cubic compound SiN_4 was predicted to be both thermodynamically and lattice-dynamically stable. Its structure consists of SiN_4 tetrahedra connected by N_2 dimers [26]. In this study, by first-principles calculations, we examined the above-mentioned proposition and half-metallicity for MN_4 (M=Mn, Fe, Co, and Ni). Our results indicate that they are all half-metals with largest spin gap up to ∼5 eV and highest $T_c \sim 10^3$ K except for Ni. We propose that the transition metals are self-doped with their 4s electrons due to the relatively low electronegativity of the N_2 dimer and the

*jgguo@iphy.ac.cn
†xlchen@iphy.ac.cn

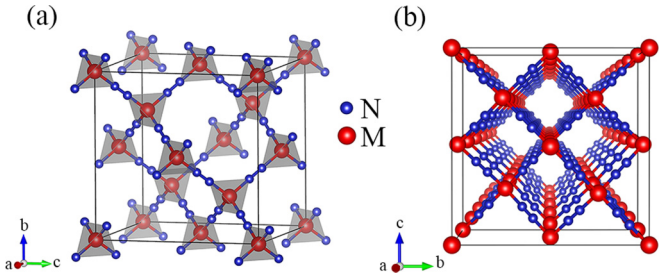

FIG. 1. (a) Crystal structure of MN_4 (M is Mn, Fe, Co), space group $Fd\bar{3}m$ (No. 227), which can be regarded as formation from the replacement of the C atoms in diamond by MN_4 tetrahedron adapted from Ref. [26]. (b) Perspective view from the [100] direction of MN_4.

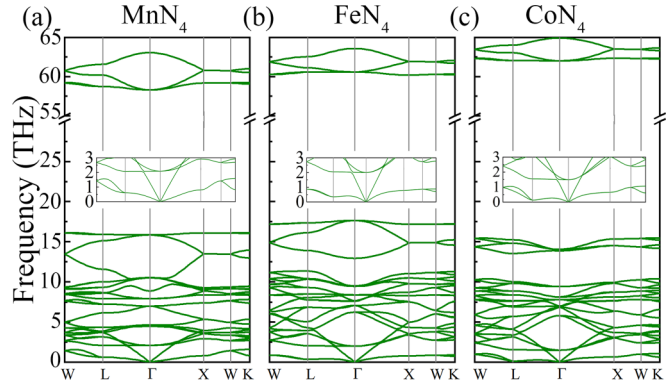

FIG. 2. Phonon spectra for (a) MnN_4, (b) FeN_4, and (c) CoN_4. The insets are zoom-in images of low frequencies of phonon spectra.

ferromagnetism arises by their spin-parallel 3d electrons in the metallic channel. In the nonmetallic channel, the large spin gaps can be attributed to the big energy difference between the bonding and antibonding states of N_2 dimers.

II. COMPUTATIONAL METHODS

Geometry optimizations, phonon spectra, and band structures were performed using the density functional theory with the generalized gradient approximation (GGA) in the form of the Perdew-Burke-Ernzerhof (PBE) [27] exchange-correlation potential implemented in CASTEP [28]. Mechanical properties and orbital resolved band structures were calculated by using the Vienna *ab initio* simulation package (VASP) [29]. The Hubbard repulsion term U was introduced to account for the correlated effects of 3d electrons. In calculation of band gaps, the HSE06 hybrid functional was adopted to enhance the accuracy. The detailed calculation methods can be found in the Supplemental Material [30].

III. RESULTS AND DISCUSSION

As described in Ref. [26], we build MN_4 with a diamond structure (space group $Fd\bar{3}m$) shown in Fig. 1(a), where M is Mn, Fe, and Co. In each unit cell, there are eight MN_4 tetrahedral units that are connected by N-N bonds. The M ions occupy the Wyckoff 8(a) site and N 32(e) site. After optimization, the M-N and N-N bond lengths are slightly shortened compared with the known compounds [12,31,32] and diazenides [33,34]. Their structural parameters are summarized in Table S1 [30].

The stability of these compounds were examined by phonon spectra, in which no negative frequencies appear, suggesting these compounds are lattice-dynamically stable, see Figs. 2(a), 2(b), and 2(c). Then we evaluate the cohesive energies E_c for MnN_4, FeN_4, and CoN_4 along with other Mn, Fe, and Co nitrides for comparison. E_c is defined as $E_c = (E_{M_xN_y} - xE_M - yE_N)/(x+y)$, where E_M, E_N, and $E_{M_xN_y}$ are the total energy of a single M atom, a single N atom, and M_xN_y compound. The results are listed in Table I. MnN_4, FeN_4, and CoN_4 are either more negative or close to E_c of the known binary compounds, indicating they are energetically stable in terms of cohesive energy. On the other hand, a convex hull analysis based on formation energy is performed. The formation energy is defined as $E_f = (E_{M_xN_y} - x\mu_M - y\mu_N)/(x+y)$, where μ_M, μ_N, and $E_{M_xN_y}$ are the total energy of stable bulk crystal M, crystal N_2, and M_xN_y compound. Figure 3, along with Table S2 [30], shows that these MN_4 are also stable. Furthermore, for a stable cubic structure, the elastic matrix should satisfy the Born stability criteria [35]: C_{11}-$C_{12} > 0$, $C_{11} + 2C_{12} > 0$, $C_{44} > 0$. The calculated C_{11}, C_{12}, and C_{44}, summarized in Table S3 [30], meet well these criteria. The structural stability of FeN_4 at elevated temperatures are examined through molecular dynamics calculations, as shown in Fig. S1 [30]. The results indicate that the structure of FeN_4 is well preserved up to 900 K.

TABLE I. Computed cohesive energies for MN_4 and known M-N compounds (M=Fe, Co, Mn).

Compounds	E_c (eV/atom)	Compounds	E_c (eV/atom)	Compounds	E_c (eV/atom)
$FeN_4(Fd\bar{3}m)$	−5.079	$CoN_4(Fd\bar{3}m)$	−5.182	$MnN_4(Fd\bar{3}m)$	−4.867
$FeN(F\bar{4}3m)$ [12]	−5.188	$CoN(F\bar{4}3m)$ [13]	−5.297	$MnN(I4/mmm)$ [14]	−4.737
$Fe_2N(Pbcn)$[15]	−4.991	$Co_2N(Pnnm)$ [16]	−5.393	$Mn_3N_2(I4/mmm)$ [17]	−4.703
$Fe_2N(P\bar{3}m1)$ [18]	−4.930	$Co_3N(P6_322)$ [19]	−5.416	$Mn_4N(Pm\bar{3}m)$ [20]	−4.009
$Fe_2N(P312)$ [21]	−5.050	$Co_4N(Pm\bar{3}m)$ [19]	−5.423		
$Fe_2N(P\bar{3}1m)$ [22]	−5.050				
$Fe_3N(P6_322)$ [23]	−5.063				
$Fe_3N(P312)$ [21]	−5.063				
$Fe_4N(Pm\bar{3}m)$ [24]	−5.015				
$Fe_8N(I4/mmm)$ [25]	−4.981				

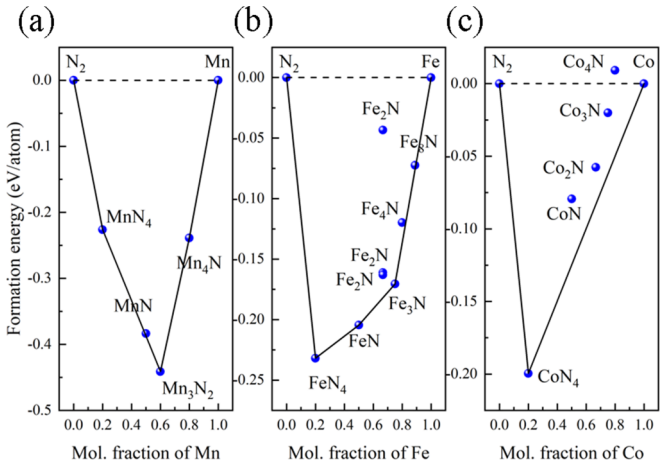

FIG. 3. Formation energies of the existing (a) Mn-N, (b) Fe-N, and (c) Co-N compounds and MN_4 (M=Mn, Fe, Co) with respect to decomposition into their elemental states. The convex hulls are shown by a solid line. The data points on the solid line means the structure is stable.

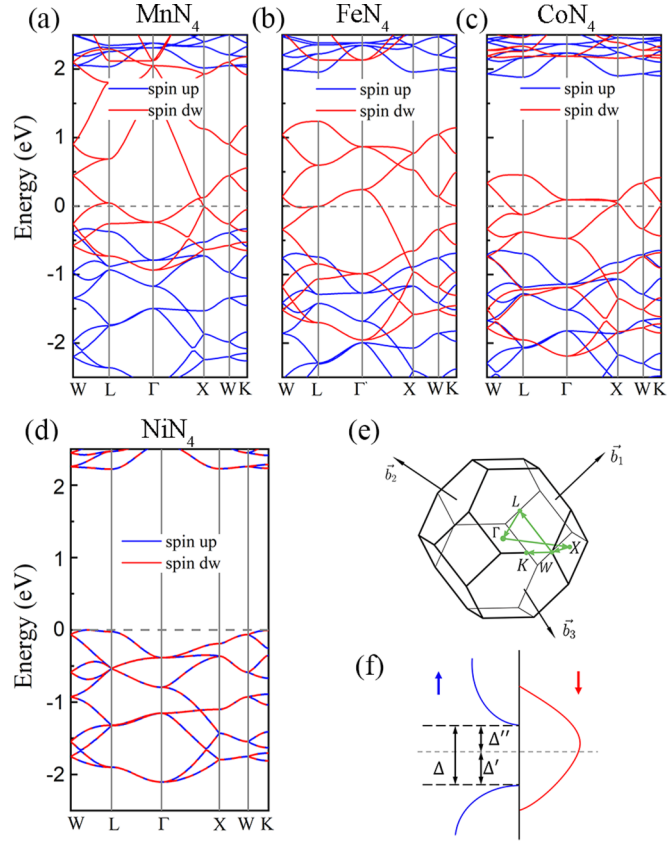

FIG. 4. Spin resolved band structures for (a) MnN_4, (b) FeN_4, (c) CoN_4, and (d) NiN_4 with a PBE functional. Blue lines denote the band structure of spin-up subband, while red lines denote the spin-down (dw) subband. (e) First Brillouin zone. (f) Spin resolved density of state schematic, spin gaps are marked as Δ, Δ', and Δ''.

The ground magnetic state of MN_4 is determined by calculating the total energies of ferromagnetic (FM), antiferromagnetic (AFM), and nonmagnetic (NM) states. The FM state is obtained from collinear spin-polarized optimization of identical spin directions of the M atoms (see Fig. S2(a) [30]). The AFM state is just reversing the nearest M spin directions in the lattice (see Fig. S2(b) [30]) and the NM state a nonspin-polarized optimization. Whether or not considering the Hubbard U term, the FM is found to be the ground state with local moment 3, 2, and 1 μ_B per formula unit for MnN_4, FeN_4, and CoN_4, respectively. The FM coupling strength, or the Curie temperature T_c, can be estimated by the mean-field approximation (MFA) through $k_B T_c^{\mathrm{MFA}} = 2\Delta E/3N$ [46], where k_B is the Boltzmann constant, N is the number of magnetic atoms in the unit cell, and ΔE is the energy difference between AFM and FM states. This formula, however, usually overestimates T_c. By using empirical relationship $T_c/T_c^{\mathrm{MFA}} = 0.8162$ [47], we correct the T_c and list them in Table II. All T_c are well above room temperature, especially for FeN_4 with $T_c = 2.70 \times 10^3$ K, much higher than that for known ferromagnets.

Figures 4(a)–4(c) show the spin resolved band structures of MN_4 (M=Mn, Fe, Co) calculated by a PBE exchange functional, where the Fermi level is set to be zero. In the spin-down subband, a metallic feature shows up. While in the spin-up subband, a semiconducting feature with varying gap emerges. The calculated T_c and gaps of MN_4 and known half-metals are summarized in Table II. Among them, FeN_4 owns the largest spin gap ~2.65 eV. The effect of the on-site Hubbard U of 3d metals should be taken into account. If we adopt $U = 3.8$ eV for Fe, a modest value as in Ref. [48], this yields a gap ~3.63 eV, see Fig. S3(b) [30]. To get a more accurate half-metallic gap for FeN_4, we performed the calculation using the HSE06 hybrid functional [see Figs. 5(a) and 5(b)] and got a spin gap $\Delta = 5.39$ eV. It is noted that the energy spans, labeled Δ' and Δ'' in Fig. 4(f), are 3.29 and 2.10 eV, respectively, which are wide enough to prevent spin-flip transitions by thermal excitations.

Apart from MnN_4, FeN_4, and CoN_4, extension to other isostructural 3d transition metals VN_4, CrN_4, and NiN_4 is tried. Again, no any negative frequencies are present in their phonon spectra for CrN_4 and NiN_4 (see Fig. S4 [30]). For VN_4, a small negative value ~0.3 THz is present near point L, which can be neglected in comparison with its large positive frequencies. In contrast, considerably negative frequencies exist for ScN_4, TiN_4, CuN_4, and ZnN_4. Among the lattice-dynamically stable structures, none is magnetic and VN_4 and CrN_4 are normal metals (Fig. S5 [30]). Of particular

TABLE II. Half-metallic gaps (PBE) and T_c for MnN_4, FeN_4, CoN_4, and known compounds.

Compounds	MnN_4	FeN_4	CoN_4	CrO_2	Sr_2FeMoO_6	NiMnSb	Fe_3O_4	Co_2FeSi
T_c (K)	1.90×10^3	2.70×10^3	8.18×10^2	386 [36]	419 [37]	730 [38]	851 [39]	1100 [40]
Gap (eV)	2.36	2.65	2.56	> 1.5 [41]	0.8 [42]	0.4 [43]	0.5 [44]	0.86 [45]

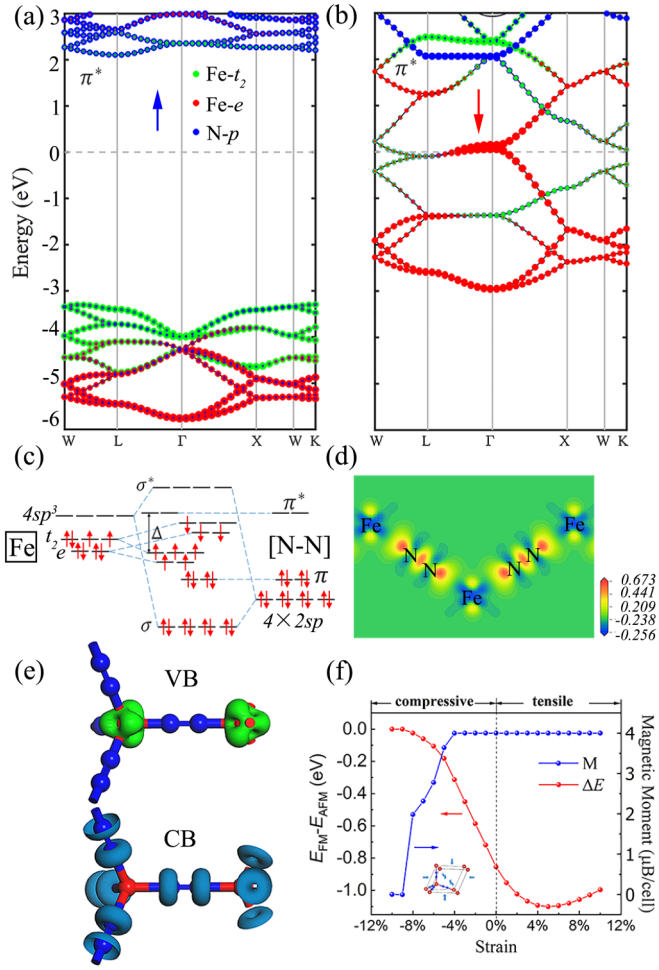

FIG. 5. Orbital resolved band structure for (a) spin up and (b) spin down of FeN_4 calculated with a HSE06 functional. Solid red and green circles represent e and t_2 orbitals for Fe atoms, and solid blue p orbitals for N atoms. The larger the circle is, the greater an orbital contributes. (c) Schematic illustration of bonding states between an Fe atom and N_2 dimers. Fe 4s electrons falls to 3d orbitals and Fe 4s, 4p orbitals hybrid with four N 2sp hybridization orbitals, leaving eight electrons in its 3d orbitals. (d) Charge density difference map for FeN_4 along the (110) plane, obtained by $\Delta\rho = \rho_{FeN_4}$-$\rho_{Fe}$-$\rho_N$. (e) Electron density of the VB (upper panel) and the CB (lower panel) for the nonmetallic channel. (f) The variation of energy difference between FM and AFM states (red) and magnetic moment (blue) under different strain.

interest, NiN_4 is a semiconductor, see Fig. 3(d). Their lattice parameters and properties are summarized in Table S1 [30].

Now we try to understand the origin of the half-metallicity of MN_4. Figures 5(a) and 5(b) show the orbital resolved band structure of nonmetallic and metallic channels for FeN_4, respectively. The 3d orbitals of Fe atoms are split into two groups, t_2 orbitals (d_{xy}, d_{yz}, d_{xz}) and e orbitals ($d_{x^2-y^2}$ and d_{z^2}), which is consistent with the situation under a tetrahedral crystal field. Apart from the sp hybrid orbitals, π and π^* orbitals are expected to form in N_2 dimers since electron density accumulations in between N-N dimers can be clearly seen in Fig. 5(d). In the nonmetallic channel, the VB are composed mainly of the Fe t_2 orbitals and the CB of the N π^* orbitals. It is noted that the energy is weakly dispersed in the VB, suggesting Fe 3d are not strongly bonded with the N_2 dimers. A similar situation occurs in the bands just above the Fermi energy in the other channel. The π bands (not shown) in both channels are far below the Fermi energy due to the wide energy separation of the π and π^* orbitals in the N_2 dimers.

Here we propose a model showing the bonding states between an Fe atom and four N_2 dimers sketched in Fig. 5(c). As the Fe atom is coordinated by four N_2 dimers, four σ bonds might form from Fe $4sp^3$ orbitals and N 2sp orbitals. Since Fe $4sp^3$ is much higher than N 2sp in energy, these electrons in the σ bonds can be totally contributed by the latter. A similar hybridization of Co-Si bond in Heusler Co_2MnSi [49] was observed. If this is true for the Fe-N σ bonds, then Fe 4s electrons can only flow into its d orbitals. That is the so-called self-doping, resulting in an Fe 3d electron configuration ↑↑↑↑↑↓↓↓, in good agreement with the calculated magnetic moment 2 μ_B per FeN_4 formula unit. More importantly, in the nonmetallic channel, the Fe 3d orbitals are fully occupied by five electrons, giving rise to a completely filled VB and an empty CB as the π^* orbitals are far higher in energy. In this way a large gap appears as labeled Δ in Fig. 5(c). The charge density shown in Fig. 5(e) confirms that the main occupancy of the Fe 3d electrons in the VB and the empty of N-N antibonding states in the CB. On the contrary, in the metallic channel, Fe 3d orbitals are only occupied by three electrons, hence the corresponding band crosses the Fermi energy.

This model could theoretically explain the integer magnetic moments for MnN_4, CoN_4, and NiN_4. Since Mn and Co have one less and one more 3d electron compared with Fe, their moments are, therefore, 3 and 1 μ_B, respectively. In both cases, their VBs are fully occupied by five 3d electrons in their nonmetallic channels. For Ni, its 3d orbitals will be occupied by eight 3d and two 4s electrons, leading to full occupations in both channels. Hence, it is a semiconductor.

Considering spin interactions in a linear Fe-N_2-Fe way, a double-exchange-like mechanism may be applicable here to establish the long-range magnetic ordering, see Fig. S6 [30]. If one spin-down electron hops from Fe 3d orbitals to the neighboring N_2 dimer π^* orbitals by thermal excitations in the metallic channel, the vacancy will be filled by one spin-down electron from another neighboring N_2 dimer. This is rather probable because these orbitals are overlapped to some extent, see Fig. 5(b). This way will help retain the spin direction and hence maintain the FM state.

The self-doping phenomena of Fe can be understood from the electronegative point of view. A N_2 dimer, as a chemical species, is quite inert and low electronegative as it meets the octet electron rule. It, however, can act as a nonmetallic element and form a variety of compounds with active metals. The reason is that a N_2 dimer has an empty π^* orbital, which can accommodate electrons from active metals. Such metals are usually alkali and alkaline-earth metals with high-enough energy s electrons. Typical examples are SrN and SrN_2 [50], both containing N_2 dimers in their structures and electrons in the π^* orbitals. Similarly, electron transfer to O_2 dimer occurs in magnetically frustrated Rb_4O_6 [51–53]. Here less active Fe has a little stronger electronegativity than Sr, whose $4s^2$ electrons are expected not to transfer to the N_2 dimers' π^* orbitals. Instead, they go to Fe's 3d orbitals, that is, the

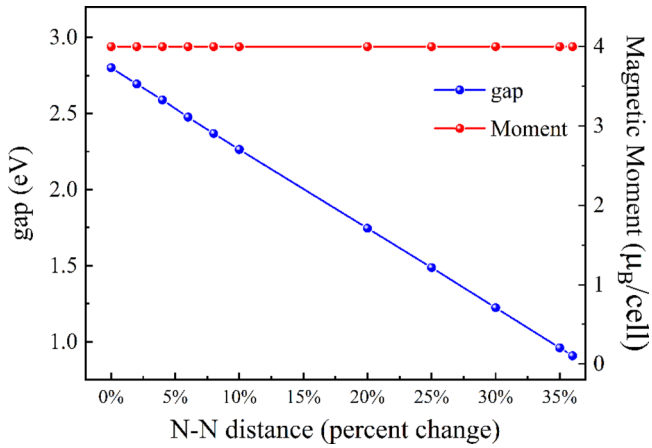

FIG. 6. The dependence of N-N distance on spin gap and magnetic moment.

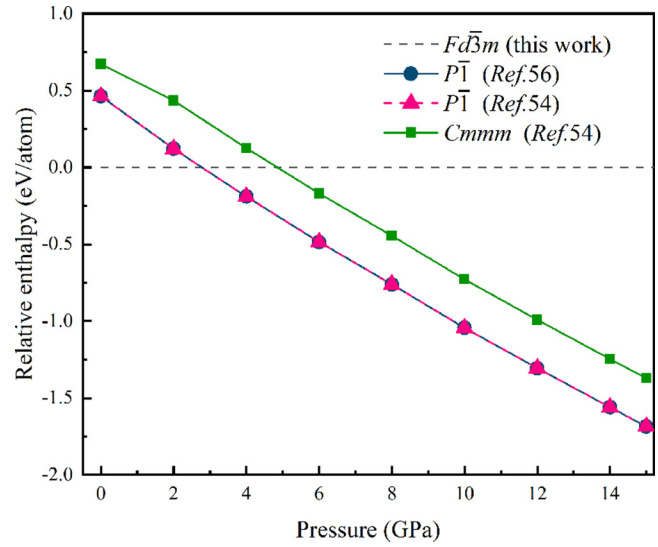

FIG. 7. Relative enthalpies of FeN_4 with different structures as a function of pressure. Cubic ($Fd\bar{3}m$) FeN_4 is taken as a standard. Negative values indicate other structures are more stable than cubic structure at a certain pressure.

self-doping of Fe. Our above calculations support that in the ground state, the π^* orbitals are unoccupied.

The robustness of half-metallicity is examined for FeN_4. Figure 5(f) shows that the magnetic moment and energy difference (E_{FM}-E_{AFM}) under strains, where the strain was simulated by $\varepsilon = (a - a_0)/a_0 \times 100\%$. The half-metallicity keeps against AFM until a tensile strain ~10%, but collapses at an ~4% compressive strain. The large spin gap depends much on the splitting of π and π^* energy level. To check the effects of N-N bond length on the spin gap of FeN_4, we enlarged the N-N distance while we kept the Fe-N distance intact. As N-N being far away, π and π^* get close to each other, resulting in decreased spin gap but a constant magnetic moment, see Fig. 6. Hence, the large spin gap originates from the appropriate bond length of N-N. These calculated results agree well with our proposition that N_2 dimers act as an electron receiver accommodated by their π^* orbitals with a reduced electronegativity. The reduced electronegativity is consistent with the self-doping phenomenon in FeN_4.

Recently, Chen *et al.* [54] predicts that FeN_4 has space groups of $P\bar{1}$ and *Cmmm* under different pressures using CALYPSO methodology [55]. Bykov *et al.* [56] synthesized another FeN_4 with space group $P\bar{1}$ by a high-pressure and laser-heating method. To compare the relative stability among them, we computed the enthalpies of them at different pressures, see Fig. 7. The results show that our diamond-like FeN_4 will transform to $P\bar{1}$ symmetry under 2.78 GPa. Hence, high pressures may not work for synthesizing the FeN_4 we predict here. But it is similar to T-carbon [57] in both structure and low density. The latter compound has been successfully synthesized by picosecond laser irradiation under a nitrogen atmosphere [58]. It might be a choice to apply similar conditions to synthesize MN_4.

IV. CONCLUSIONS

By first-principles calculations, we predicted three half-metals MnN_4, FeN_4, and CoN_4. They crystallize in a diamondlike structure with space group $Fd\bar{3}m$. They are not only favored in energy, lattice-dynamically, and mechanically stable, but also possess robust FM coupling with the highest Curie temperature $T_c \sim 10^3$ K. Band structures indicate the largest spin gap is around 5 eV (HSE06). The proposition of self-doping of these 3*d* transition metals caused by the reduction in electronegativity of N_2 dimers, well explains the calculated integer magnetic moments of MN_4. The N_2 dimer plays an important role in enlarging the spin gap for half-metal MN_4 (M=Mn, Fe, Co). Other emergent magnetic properties are expected in compounds consisting of *d* metals and N_2 dimers with modified structures.

ACKNOWLEDGMENTS

This work is financially supported by the National Natural Science Foundation of China under Grants No. 51532010 and No. 51772322; the National Key Research and Development Program of China (2016YFA0300600, 2017YFA0304700); and the Key Research Program of Frontier Sciences, CAS, Grant No. QYZDJ-SSW-SLH013.

[1] R. A. de Groot, F. M. Mueller, P. G. vanEngen, and K. H. J. Buschow, Phys. Rev. Lett. **50**, 2024 (1983).

[2] Y. Lu, X. W. Li, G. Q. Gong, G. Xiao, A. Gupta, P. Lecoeur, J. Z. Sun, Y. Y. Wang, and V. P. Dravid, Phys. Rev. B **54**, R8357(R) (1996).

[3] M. Viret, M. Drouet, J. Nassar, J. P. Contour, C. Fermon, and A. Fert, Europhys. Lett **39**, 545 (1997).

[4] G. Schmidt and L. W. Molenkamp, Semicond. Sci. Technol. **17**, 310 (2002).

[5] H. C. Kandpal, G. H. Fecher, and C. Felser, J. Phys. D **40**, 1507 (2007).

[6] I. Galanakis, P. Mavropoulos, and P. H. Dederichs, J. Phys. D **39**, 765 (2006).

[7] M. A. Korotin, V. I. Anisimov, D. I. Khomskii, and G. A. Sawatzky, Phys. Rev. Lett. **80**, 4305 (1998).

[8] A. Yanase and K. Siratori, J. Phys. Soc. Jpn **53**, 312 (1984).

[9] K. L. Kobayashi, T. Kimura, H. Sawada, K. Terakura, and Y. Tokura, Nature (London) **395**, 677 (1998).

[10] D. D. Sarma, P. Mahadevan, T. Saha-Dasgupta, S. Ray, and A. Kumar, Phys. Rev. Lett. **85**, 2549 (2000).

[11] M. I. Katsnelson, V. Y. Irkhin, L. Chioncel, A. I. Lichtenstein, and R. A. de Groot, Rev. Mod. Phys. **80**, 315 (2008).

[12] K. Suzuki, H. Morita, T. Kaneko, H. Yoshida, and H. Fujimori, J. Alloys Compd. **201**, 11 (1993).

[13] K. Suzuki, T. Kaneko, H. Yoshida, H. Morita, and H. Fujimori, J. Alloys Compd. **224**, 232 (1995).

[14] K. Suzuki, T. Kaneko, H. Yoshida, Y. Obi, H. Fujimori, and H. Morita, J. Alloys Compd. **306**, 66 (2000).

[15] D. Rechenbach and H. Jacobs, J. Alloys Compd. **235**, 15 (1996).

[16] M. Hasegawa and T. Yagi, J. Alloys Compd. **403**, 131 (2005).

[17] G. Kreiner and H. Jacobs, J. Alloys Compd. **183**, 345 (1992).

[18] Z. Pinsker, and S. Kaverin, Dokl. Akad. Nauk SSSR **96**, 519 (1954).

[19] M. Lourenço, M. Carvalho, P. Fonseca, T. Gasche, G. Evans, M. Godinho, and M. Cruz, J. Alloys Compd. **612**, 176 (2014).

[20] R. Juza, K. Deneke, and H. Puff, Z. Elektrochem. **63**, 551 (1959).

[21] K. H. Jack, Acta Crystallogr. **5**, 404 (1952).

[22] A. Burdese, Metall. Ital. **3**, 195 (1957).

[23] A. Leineweber, H. Jacobs, F. Hüning, H. Lueken, H. Schilder, and W. Kockelmann, J. Alloys Compd. **288**, 79 (1999).

[24] H. Jacobs, D. Rechenbach, and U. Zachwieja, J. Alloys Compd. **227**, 10 (1995).

[25] M. Widenmeyer, L. Shlyk, A. Senyshyn, R. Münig, and R. Niewa, Z. Anorg. Allg. Chem **641**, 348 (2015).

[26] N. Liu, X. Chen, J. Guo, J. Deng, and L. Guo, Chin. Phys. Lett. **35**, 087102 (2018).

[27] J. P. Perdew, K. Burke, and M. Ernzerhof, Phys. Rev. Lett. **77**, 3865 (1996).

[28] S. J. Clark, M. D. Segall, C. J. Pickard, P. J. Hasnip, M. J. Probert, K. Refson, and M. C. Payne, Z. Kristallogr. Cryst. Mater. **220**, 567 (2005).

[29] G. Kresse and J. Furthmüller, Phys. Rev. B **54**, 11169 (1996).

[30] See Supplemental Material at http://link.aps.org/supplemental/10.1103/PhysRevB.99.184409 for lattice parameters, formation energies, elastic constants, MD simulation, magnetic configurations, band structure, phonon spectra, and computational details, which includes Refs. [59–71].

[31] A. Gazhulina and M. Marychev, J. Alloys Compd. **623**, 413 (2015).

[32] Z. T. Y. Liu, X. Zhou, S. V. Khare, and D. Gall, J. Phys. Condens. Matter **26**, 025404 (2014).

[33] G. V. Vajenine, G. Auffermann, Y. Prots, W. Schnelle, R. K. Kremer, A. Simon, and R. Kniep, Inorg. Chem. **40**, 4866 (2001).

[34] G. Auffermann, Y. Prots, and R. Kniep, Angew. Chem. Int. Ed. **40**, 547 (2001).

[35] F. Mouhat and F. X. Coudert, Phys. Rev. B **90**, 224104 (2014).

[36] H. Huang, K. Seu, A. Reilly, Y. Kadmon, and W. F. Egelhoff, J. Appl. Phys. **97**, 10C309 (2005).

[37] F. K. Patterson, C. W. Moeller, and R. Ward, Inorg. Chem. **2**, 196 (1963).

[38] C. N. Borca, T. Komesu, H.-K. Jeong, P. A. Dowben, D. Ristoiu, C. Hordequin, J. P. Nozières, J. Pierre, S. Stadler, and Y. U. Idzerda, Phys. Rev. B **64**, 052409 (2001).

[39] D. Gubbins and E. Herrero-Bervera, *Encyclopedia of Geomagnetism and Paleomagnetism* (Springer Science & Business Media, New York, 2007), p. 23.

[40] S. Wurmehl, G. H. Fecher, H. C. Kandpal, V. Ksenofontov, C. Felser, H.-J. Lin, and J. Morais, Phys. Rev. B **72**, 184434 (2005).

[41] P. Schlottmann, Phys. Rev. B **67**, 174419 (2003).

[42] H. P. Xiang, Z. J. Wu, and J. Meng, Phys. Status Solidi B **242**, 1414 (2005).

[43] C. Felser and A. Hirohata, *Heusler Alloys* (Springer, Berlin, 2015), p. 10.

[44] H.-T. Jeng and G. Y. Guo, Phys. Rev. B **65**, 094429 (2002).

[45] R. Mohankumar, S. Ramasubramanian, M. Rajagopalan, M. Manivel Raja, S. V. Kamat, and J. Kumar, J. Mater. Sci **50**, 1287 (2015).

[46] H. Jin, Y. Dai, B. Huang, and M.-H. Whangbo, Appl. Phys. Lett. **94**, 162505 (2009).

[47] N. W. Ashcroft and N. D. Mernin, *Solid State Physics* (Holt. Rinehart and Winston, New York, 1976), p. 717.

[48] R. Bliem, J. Pavelec, O. Gamba, E. McDermott, Z. Wang, S. Gerhold, M. Wagner, J. Osiecki, K. Schulte, M. Schmid, P. Blaha, U. Diebold, and G. S. Parkinson, Phys. Rev. B **92**, 075440 (2015).

[49] T. Graf, C. Felser, and S. S. P. Parkin, Prog. Solid State Chem. **39**, 1 (2011).

[50] O. Volnianska and P. Boguslawski, Phys. Rev. B **77**, 220403(R) (2008).

[51] J. Winterlik, G. H. Fecher, C. A. Jenkins, C. Felser, C. Mühle, K. Doll, M. Jansen, L. M. Sandratskii, and J. Kübler, Phys. Rev. Lett. **102**, 016401 (2009).

[52] J. J. Attema, G. A. de Wijs, G. R. Blake, and R. A. de Groot, J. Am. Chem. Soc. **127**, 16325 (2005).

[53] J. Winterlik, G. H. Fecher, C. Felser, C. Mühle, and M. Jansen, J. Am. Chem. Soc. **129**, 6990 (2007).

[54] Y. Chen, X. Cai, H. Wang, H. Wang, and H. Wang, Sci. Rep. **8**, 10670 (2018).

[55] Y. Wang, J. Lv, L. Zhu, and Y. Ma, Phys. Rev. B **82**, 094116 (2010).

[56] M. Bykov, E. Bykova, G. Aprilis, K. Glazyrin, E. Koemets, I. Chuvashova, I. Kupenko, C. McCammon, M. Mezouar, V. Prakapenka, H. P. Liermann, F. Tasnádi, A. V. Ponomareva, I. A. Abrikosov, N. Dubrovinskaia, and L. Dubrovinsky, Nat. Commun. **9**, 2756 (2018).

[57] X.-L. Sheng, Q.-B. Yan, F. Ye, Q.-R. Zheng, and G. Su, Phys. Rev. Lett. **106**, 155703 (2011).

[58] J. Zhang, R. Wang, X. Zhu, A. Pan, C. Han, X. Li, Z. Dan, C. Ma, W. Wang, H. Su, and C. Niu, Nat. Commun. **8**, 683 (2017).

[59] A. Jain, S. P. Ong, G. Hautier, W. Chen, W. D. Richards, S. Dacek, S. Cholia, D. Gunter, D. Skinner, G. Ceder, and K. A. Persson, APL Mater. **1**, 011002 (2013).

[60] V. Stevanović, S. Lany, X. Zhang, and A. Zunger, Phys. Rev. B **85**, 115104 (2012).

[61] L. Wang, T. Maxisch, and G. Ceder, Phys. Rev. B **73**, 195107 (2006).
[62] K. Persson, Materials Data on N2 (SG:205) by Materials Project (2014).
[63] J. F. Nye, *Physical Properties of Crystals: Their Representation by Tensors and Matrices* (Oxford University Press, Oxford, 1985), pp. 146–147.
[64] E. W. Kammer, T. E. Pardue, and H. F. Frissel, J. Appl. Phys. **19**, 265 (1948).
[65] A. Reuss, Z. Angew. Math. Mech **9**, 49 (1929).
[66] R. Hill, Proc. Phys. Soc. London. Sec. A **65**, 349 (1952).
[67] N. S. E. Schreiber and O. L. Anderson, *Elastic Constants and Their Measurement* (McGraw-Hill, New York, 1974), pp. 29–31.
[68] H. J. Monkhorst and J. D. Pack, Phys. Rev. B **13**, 5188 (1976).
[69] B. G. Pfrommer, M. Cote, S. G. Louie, and M. L. Cohen, J. Comput. Phys. **131**, 233 (1997).
[70] G. Kresse and D. Joubert, Phys. Rev. B **59**, 1758 (1999).
[71] A. Jain, G. Hautier, S. P. Ong, C. J. Moore, C. C. Fischer, K. A. Persson, and G. Ceder, Phys. Rev. B **84**, 045115 (2011).